Medicinal Chemistry

International Edition: DOI: 10.1002/anie.201601147
German Edition: DOI: 10.1002/ange.201601147

Generalizing the Concept of Specific Compound Formulation Additives towards Non-Fluorescent Drugs: A Solubilization Study on Potential Anti-Alzheimer-Active Small-Molecule Compounds

Carmen Lawatscheck, Marcus Pickhardt, Sebastian Wieczorek, Andrea Grafmüller, Eckhard Mandelkow, and Hans G. Börner**

Abstract: *Tailor-made compound formulation additives enable the testing of potential drugs with undesirable pharmacological profiles. A combinatorial approach using Raman microscopy as the readout method is presented to select peptide sequences from large one-bead-one-compound libraries. The resulting peptide–PEG conjugates solubilize potential prophylactic and therapeutic anti-Alzheimer compounds and can be used as specific additives not only for fluorescent but also for non-fluorescent compounds.*

Considerable efforts and resources are devoted in both academic and industrial research to develop new drug entities.[1] Statistically, out of 10^4 potentially disease-modifying compounds entering preclinical studies, five to ten are evaluated closely, leading to one or two products.[2] Highly lipophilic, small-molecule lead compounds have received particular interest, which has, however, resulted in high numbers of early-stage drug-structure rejections owing to their poor water solubility and low bioavailability.[3] Thus effective strategies for the direct testing of lead compounds that do not require resource-intensive structure-adaption cycles to improve water solubility are needed.[4]

Common approaches involve compound solubilization by using formulation additives.[5] At early drug-evaluation stages, dimethyl sulfoxide (DMSO) is often used.[6] Block copolymers, on the other hand, do not only increase the solubility and bioavailability but also contribute to the drug stability and the realization of advanced functions, for example, barrier translocation, controlled release, or tissue targeting.[7]

Recently, the concept of specific formulation additives was introduced for improving the pharmaceutical properties of bioactive compounds.[8] Peptide–polymer conjugates offer interesting opportunities for biomedical applications[9] and were used to render difficult, small organic drug molecules water-soluble.[10] While the peptide controls the selective uptake of the drug, a poly(ethylene glycol) (PEG) block provides solubility and shielding. Peptide–PEG conjugates can be used for biotesting and increase the bioavailability of insoluble drugs as shown for a set of kinase IpsE inhibitors and the photosensitizer *meta*-tetra(hydroxyphenyl)chlorin (*m*-THPC).[8,10]

A combinatorial strategy using fluorescence microscopy enabled the selection of *m*-THPC-binding peptides from large one-bead-one-compound peptide libraries. The corresponding peptide–PEG conjugates showed superior drug solubilization properties, and the release kinetics could be adjusted or the release even triggered by external stimuli.[11] However, only a minor fraction of lead structures are suitable for the florescence-based selection process. Hence the extension of the concept towards non-fluorescent entities is mandatory.

Herein, we present a more generic approach that exploits Raman microscopy to follow the partitioning of non-fluorescent small-molecule compounds in peptide libraries to select peptidic drug binders (Figure 1). Proof of principle was demonstrated by identifying specific formulation additives for B4A1, a potential anti-Alzheimer disease (anti-AD) compound that prevents Tau protein aggregation.[12] The resulting peptide–PEG conjugates enhanced the bioavailability of the compound in in vitro studies, making DMSO obsolete and offering means to investigate difficult compounds at this early stage.[13]

Current approaches for AD treatment focus primarily on alleviating the symptoms.[14] However, insight into the molecular basis of AD revealed that apart from the pathologic plaque formation by the β-amyloid peptide, abnormal changes in the Tau protein that lead to its aggregation to neurotoxic paired helical filaments are the main reason for the progression of the disease.[15] Promising strategies to advance anti-AD drugs for preventive or therapeutic treatment focus on the development of Tau aggregation inhibitors.[12] Aside from rhodanine and phenylthiazolyl hydrazide derivatives,[16] the compound B4A1 was identified in an in vitro screening as an active Tau aggregation inhibitor and

[*] C. Lawatscheck, S. Wieczorek, Prof. Dr. H. G. Börner
Humboldt-Universität zu Berlin
Department of Chemistry
Brook-Taylor-Strasse 2, 12489 Berlin (Germany)
E-mail: h.boerner@HU-Berlin.de
Dr. M. Pickhardt, Prof. Dr. E. Mandelkow
German Center for Neurodegenerative Diseases (DZNE)
CAESAR Research Center
Ludwig-Erhard-Allee 2, 53175 Bonn (Germany)
Dr. A. Grafmüller
Max Planck Institute of Colloids and Interfaces
Department of Theory and Biosystems
Am Mühlenberg 1, 14476 Potsdam (Germany)
Prof. Dr. E. Mandelkow
MPI for Metabolism Research, Hamburg Outstation, c/o DESY
Notkestrasse 85, 22607 Hamburg (Germany)

Supporting information for this article (materials, instrumentation, experimental procedures, and analytical data) can be found under: http://dx.doi.org/10.1002/anie.201601147.

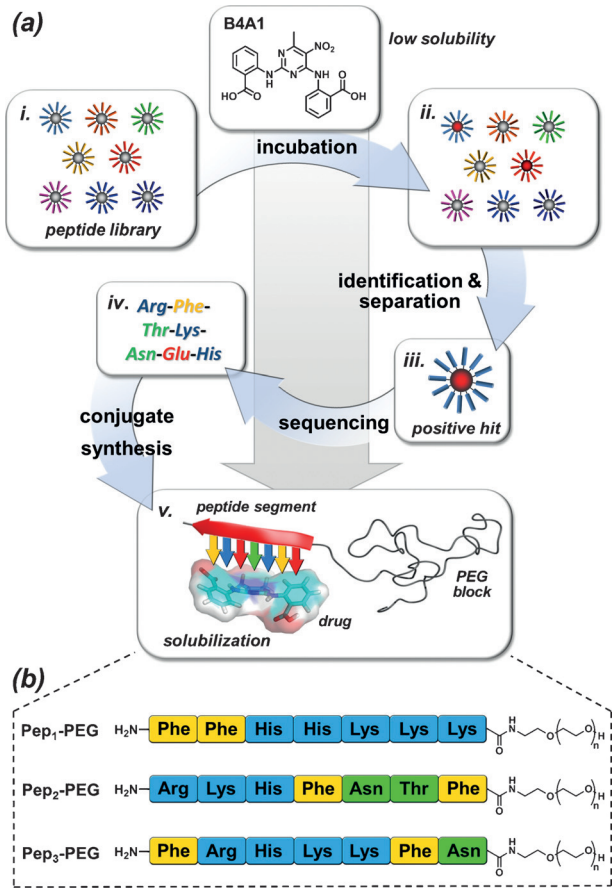

Figure 1. Design of specific solubilizers for the non-fluorescent potential drug B4A1. a) Incubation of a one-bead-one-compound peptide library (i) with B4A1 can be followed by Raman microscopy (ii) to identify compound-enriched beads (iii), and single-bead sequencing reveals peptides with high B4A1 binding capacities (iv). The synthesis of solubilizing peptide–PEG conjugates (v) leads to (Pep_1–Pep_3)–PEG (b), which render B4A1 water-soluble.

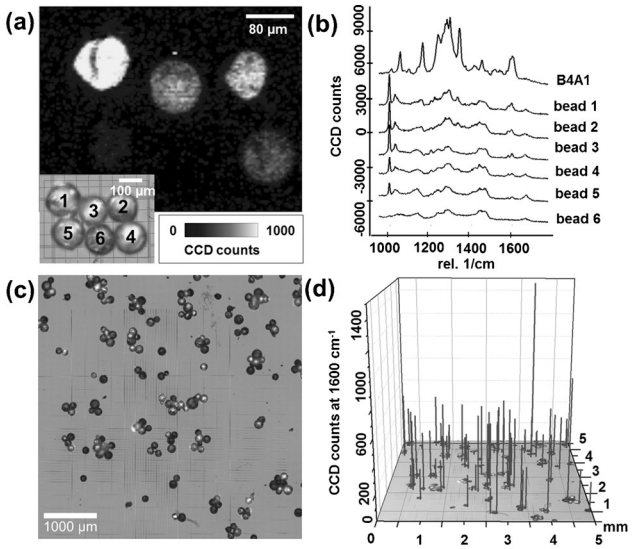

Figure 2. Raman microcopy analysis of the B4A1 enrichment of peptide-functionalized supports to identify beads with high capacities. a) Large-area Raman scan showing the intensities of the B4A1 characteristic band at 1600 cm^{-1} (inset: optical micrograph). b) Corresponding full Raman spectra of the beads. c) Optical microscopy image of one subset of incubated library beads. d) Visualized screening analysis showing the intensities of the 1600 cm^{-1} band for each individual bead, measured by "AutoFocus" single-spectrum analysis, 2×2 s per spectrum.

deaggregator of Tau aggregates in cell-free models. However, the new entity suffers from poor solubility.[17]

To select tailor-made peptide sequences with high affinity to B4A1, a one-bead-one-compound peptide library covering a sequential space of 7^7 different heptamer peptides was synthesized on ChemMatrix resin by split-and-mix procedures.[18] Considering the compound structure, the amino acids L-Arg, L-Lys, L-His, and L-Glu were chosen to enable ion pair interactions, L-Phe was chosen to provide van der Waals and π contacts, and L-Thr and L-Asn were used to establish polar interactions and hydrogen bonding. For facile single-bead sequencing, a Gly–Gly–Met segment was incorporated as a cyanogen bromide cleavable linker between the variable peptide section and the support. The library of fully deprotected peptides was incubated overnight with a 2.7 mM solution of B4A1 in DMSO/water (4:5, v/v), enabling the rapid partitioning of the barely soluble compound. After intense washing, the incubated beads were placed on a glass slide, and the solvent was removed before the system was analyzed by optical microscopy (Figure 2).

The B4A1 enrichment at beads presenting suitable peptide sequences could be followed by Raman microscopy with a $\lambda = 785$ nm laser. The Raman spectra of B4A1 contained an intense vibration band at 1600 cm^{-1}, which was attributed to an asymmetric CC stretching mode of the aromatic ring system of B4A1 and served as a suitable reference (Figure 2).[19] A high-resolution scan of six different beads confirmed that for B4A1, low- and high-capacity beads could be distinguished (Figure 2a,b). A larger set of beads was analyzed by the AutoFocus procedure, acquiring only one spectrum for the center of each bead. This method reduces the sample time and assures that the Raman band intensities can be compared owing to the optimized focus (Figure 2c,d; see also Figure S3 in the Supporting Information). Consequently, a trigger intensity of > 1000 CCD counts at 1600 cm^{-1} was chosen to identify beads with high B4A1 enrichment. Forty positive hits could be identified by this approach, and single-bead sequencing by MALDI-TOF-MS/MS revealed 30 sequences (Table S1). Considering the cargo structure, it appears to be consistent that the identified peptides were rich in Phe and basic residues. Apparently, π–π stacking and Coulombic interactions dominate B4A1–peptide binding. Interestingly, the basic residues occur mostly in blocks of three to five amino acids next to Phe. Asn and Thr, on the other hand, form hydrogen bonds, for example, with the polar diamine-pyrimidine core of B4A1. For detailed solubilization and application studies, three of the identified sequences were synthesized as peptide–PEG conjugates ((Pep_1–Pep_3)–PEG). The selected peptide sequences all contain a block segment of cationic residues, but differ in the positioning of the Phe residues. Whereas Pep_1–PEG contains a Phe–Phe diade, Pep_2–PEG features a polar Asn–Thr spacer in the aromatic

segment, and in Pep_3—PEG, the two Phe residues are positioned as flanking units of the cationic block. Solid-phase peptide synthesis following an inverse conjugation strategy yielded conjugates with PEG of $M_n = 3200$.[20] After detachment from the support, the deprotected conjugates were isolated. Mass spectrometry and NMR spectroscopy confirmed the chemical structures of (Pep_1–Pep_3)–PEG (see the Supporting Information).

All conjugates were readily soluble in water and acted as potent formulation additives, improving the water solubility of B4A1 compared to solubilization experiments with PEG or pure water (Figure S9). UV/Vis spectroscopy at 384 nm provided insight into the maximum payload capacities.[10] The capacity clearly depends on the peptide sequence. Whereas with Pep_1–PEG and Pep_2—PEG, high payloads of 0.83 mmol and 0.94 mmol drug per mmol carrier, respectively, were achieved, Pep_3–PEG reached 0.65 mmol drug per mmol carrier. These payloads are even five to seven times higher than those achieved with Cremophor ELP.[21] This clinically used formulation additive could only solubilize 0.13 mmol of B4A1 per mmol of Cremophor, which highlights the effectiveness of the new solubilizers.

A closer evaluation of the amino acid sequences suggests that a blockwise occurrence of cationic and aromatic residues in the peptide is favorable, and that a flexible, polar spacer between the two Phe residues contributes to optimized binding contacts. Remarkably, a nearly stoichiometric molar B4A1/carrier ratio of $1{:}1.1 \pm 0.1$ could be reached with Pep_2–PEG. Hence, the carrier improves compound availability by a factor of approximately 20 compared to its solubility in pure water. The other additives also showed very satisfactory molar ratios of $1{:}1.2 \pm 0.1$ and $1{:}1.5 \pm 0.4$ for Pep_1–PEG and Pep_3–PEG, respectively. To understand the sequence dependency of the carrier capacities, idealized 1:1 complexes of B4A1 and the peptide binding domains (Pep_1–Pep_3) were simulated (Figure 3; see also Figures S10 and S11).

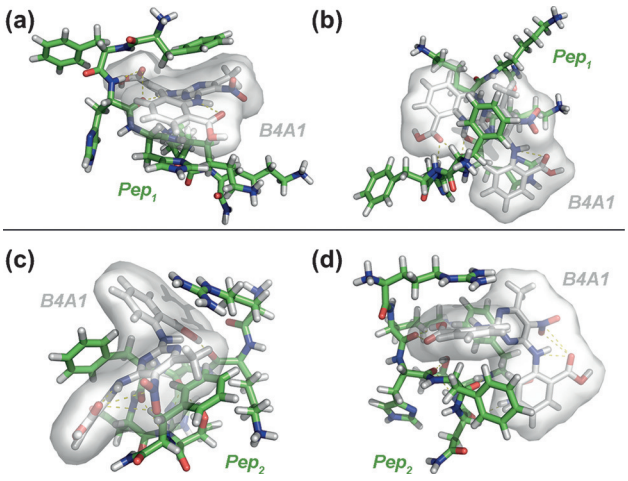

Figure 3. Representative snapshots from the MD simulations of B4A1 (shown as the van der Waals surface) binding to tailored peptide sequences (shown as sticks) in idealized 1:1 complexes: Pep_1/B4A1 (top), Pep_2/B4A1 (bottom). Side views (a, c) and top views (b, d); the simulations were visualized with PyMOL.

All three peptide sequences show considerable binding to B4A1 during the simulations. The model complexes are rather dynamic in nature as indicated by the interaction energies of −200, −150, and −180 kJ mol^{-1} for Pep_1/B4A1, Pep_2/B4A1, and Pep_3/B4A1, respectively. Analysis of the two most effective solubilizers revealed that in general, Pep_2/B4A1 complexes exhibit more conformations that are equal in energy than Pep_1/B4A1. Pep_2 was expected to have a higher conformational freedom because of the spacer between Phe_1 and Phe_4. The simulations indicate several intra- and intermolecular interactions between the drug and the peptides, and representative snapshots are shown in Figure 3. Statistically, π–π interactions dominate the contacts, with an average of 1.3 and 1.4 π–π interactions in Pep_1/B4A1 and Pep_2/B4A1, respectively. Pep_1 interacts with B4A1 mostly through π contacts between one Phe residue and the central pyrimidine ring of B4A1 (80% parallel and 20% perpendicular interactions). Further π interactions between either of the His residues and an aminobenzoic acid group of B4A1 were also observed. Hydrogen bonds were formed between the peptidic backbone and both the secondary amine and the carboxylic acid groups of B4A1. Interestingly, Phe_2 and the three lysine residues often bend away from the compound to interact with the solvent. The binding modes of Pep_2 and B4A1 indicate π–π interactions between the pyrimidine unit of B4A1 and one Phe residue (65–75% parallel and 25–35% perpendicular interactions). Furthermore, in the displayed conformation, one aminobenzoic acid segment is sandwiched between Phe_4 and Arg_1, and T-shaped π–π stacking and cation–π interactions were clearly observed. Hydrogen bonds are formed between the carboxylic acid moiety of B4A1 and the peptidic backbone. The complex is further stabilized by intrapeptidic hydrogen bonds involving the side chain of Thr_6 and amide groups of the peptidic backbone.

In general, separating the two Phe residues in Pep_2 with two polar amino acids provided additional flexibility. The same applies to Arg_1 and Phe_4, which are separated by Lys_2–His_3. These spacings enable Pep_2 to complex B4A1 in a more dynamic fashion compared to the binding modes of the Pep_1/B4A1 complex. The blockwise arrangement of aromatic and cationic residues in Pep_1 appears to be less favorable for cargo binding. Despite the fact that the revealed binding interactions only have model character, the findings are consistent with the solubilization experiments, where Pep_1–PEG showed a lower capacity than Pep_2–PEG. Hence, the interaction modes observed within these complexes are even more likely to also occur in the actual B4A1/carrier complexes. For comparison, simulations were performed for the Pep_3/B4A1 complex as well, which showed the lowest capacity for conjugate solubilization. Although this is not expressed in the interaction energy, which lies in between those of Pep_1/B4A1 and Pep_2/B4A1, the simulations are consistent with Pep_3 having the lowest B4A1 binding capacity. Cation–π interactions between Arg_2 and B4A1 could be observed, but Phe_1, which is located next to Arg_2 on the N terminus, is apparently not involved in the binding as it faces the solvent without being in contact with B4A1 (see Figure S13). Thus only one of the Phe residues interacts with B4A1, leading to an overall average of 1.0 π–π interactions. Furthermore, the

His–Lys–Lys segment is facing away from B4A1. Therefore, the main interactions between Pep_3 and B4A1 are those involving Arg_2 and Phe_6 but the parallel aromatic π–π interaction is often slightly shifted and thus most likely not as strong as in Pep_1/B4A1 and Pep_2/B4A1.

Dynamic light scattering (DLS) experiments confirmed the formation of colloidal aggregates during loading with B4A1 for all PEG–peptide additives. Whereas all PEG–peptide conjugates are molecularly dissolved prior to cargo loading, the Pep_1–PEG/B4A1, Pep_2–PEG/B4A1, and Pep_3–PEG/B4A1 complexes had hydrodynamic radii (R_h) of 105, 175, and 110 nm, respectively. This cargo-induced aggregation was expected to occur considering the low solubility and the chemical structure of B4A1, which allows for multi-point interactions with the peptide hosts. Drug-induced aggregation is advantageous as it facilitates the clearance of the carrier from a biosystem after cargo unloading. Such a mechanism is not obvious for Cremophor. Owing to its strongly amphiphilic nature, the additive forms aggregates in water with $R_h = 12$–13 nm prior to and after B4A1 loading. The quantification of the compound–transporter interactions by measuring the dissociation constants (K_D) would be of importance here, but the reliable determination of K_D values remains difficult owing to the complexity of the system.

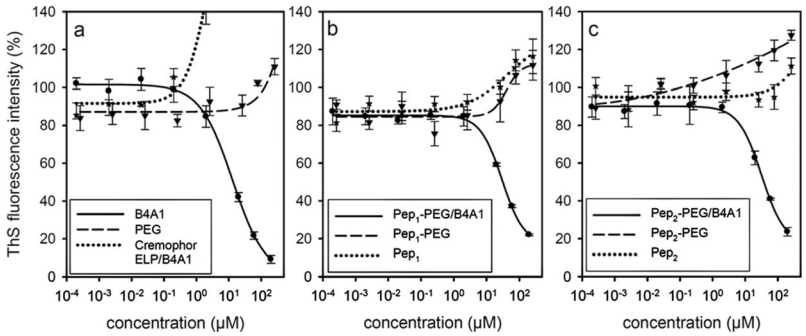

Figure 4. B4A1 activity towards the disassembly of Tau^{3RD} aggregates with and without tailored formulation additives as determined by in vitro ThS assays. The remaining ThS fluorescence after incubation in the presence of B4A1 and PEG (a), peptides Pep_1 and Pep_2 (b, c), the conjugates Pep_1–PEG and Pep_2–PEG (b, c), or the complexes Pep_1–PEG/B4A1 and Pep_2–PEG/B4A1 (b, c) was plotted as a percentage of the untreated control.

Successful drug formulation additives should not only enable effective compound solubilization, but also be of low toxicity and ensure compound availability to act on the targeted bioprocesses. Prior to studying the impact of the carriers on the B4A1 activity, the effect of the compound–transporter complexes on cell apoptosis was determined by an Annexin V test (see Figure S17). Neuroblastoma-2a (N2a) cell lines, which express $Tau^{4RD}\Delta K280$ proteins, are established reference cell systems for Alzheimer therapy approaches. The N2a cells were incubated with B4A1 or the solubilizer/B4A1 complexes, and apoptic cells were labeled with Annexin V. In comparison with the reference, which led to 16% apoptosis, in the presence of all bioconjugate carriers and the (Pep_1–Pep_3)–PEG/B4A1 complexes, significantly reduced apoptosis was observed (8–12%; see Figure S10). Interestingly, the cremophor/B4A1 complexes induced by far the highest apoptosis rate (55%), which might be due to the large amount of carrier that results from the low payload. Thr peptide–PEG conjugates and their drug complexes thus seem to be significantly less toxic than the cremophor ELP complexes.

The two most promising complexes, Pep_1–PEG/B4A1 and Pep_2–PEG/B4A1, were then further evaluated to determine their activity to disaggregate Tau protein agglomerates. In in vivo studies, the cargo/transporter complexes have to facilitate the entry of B4A1 into neuronal brain cells, which involves the crossing of the blood–brain barrier and the cell membrane. However, a capable in vitro assay was recently established that enables the rapid evaluation of compound activity by dose-dependent thioflavin S (ThS) fluorescence analysis and monitors the disassembly of preformed K19–Tau aggregates (Tau^{3RD}, the "repeat domain" of Tau responsible for aggregation).[22]

Cell-free models containing aggregated Tau^{3RD} plaques showed an effective reduction of the THS fluorescence with increasing concentrations of solubilized B4A1. Highly promising half-maximum compound concentrations for the disassembly of Tau aggregates (DC_{50}) were found, namely 31.1 ± 1.1 μM and 37.5 ± 3.0 μM for Pep_1–PEG/B4A1 and Pep_2–PEG/B4A1, respectively (Figure 4). Cremophor/B4A1, on the other hand, induced the further aggregation of Tau proteins, probably owing to the stronger amphipathic nature of the solubilizer, and thus no DC_{50} value could be determined. Moreover, compound B4A1 alone had no measurable activity in analogous DMSO-free assays owing to its poor water solubility and low availability. Control experiments showed that neither PEG nor the peptides nor the PEG–peptide conjugates had a significant effect on Tau disaggregation (Figure 4). Apparently, the tailored additives were able to release the active compound to promote the disassembly of Tau aggregates. Assays under equivalent conditions, but with DMSO instead of the bioconjugates to solubilize B4A1, confirmed the high potency of B4A1. The observed DC_{50} value of 13.5 ± 1.9 μM is slightly smaller than those of the PEG–peptide formulation additives. However, all DC_{50} values are in a comparable, low-micromolar range. It should be taken into account that for the DMSO-solubilized B4A1, the drug and the Tau protein aggregates can directly interact, whereas in the case of the Pep–PEG/B4A1 complexes, a competitive equilibrium between B4A1, the peptide binding domain, and the Tau protein is to be expected. This might account for the increased DC_{50} values found for these B4A1-loaded complexes. However, taking recent concerns that DMSO-containing stock solutions might have an effect on relevant protein functions during drug testing into account, alternative solubilizer systems and DMSO-free assays will be mandatory for early-stage drug discovery.[6]

To confirm the versatility of this generic concept, peptide–PEG solubilizers were also developed for BB14, a structurally different anti-AD compound with poor solubility (see the Supporting Information).[16a] The optimized procedure pro-

vided a set of drug-binding peptides (Table S5). Among these peptides, three solubilizers exhibiting structural similarities were synthesized as peptide–PEG conjugates ((Pep_4–Pep_6)–PEG). The highest payload was found for Pep_6–PEG, which solubilized 0.09 mmol of BB14 per mmol of the conjugate.

In conclusion, a combinatorial screening procedure was complemented with confocal Raman microscopy to identify peptides for tailor-made formulation additives based on PEG–peptide conjugates to render the non-fluorescent anti-Alzheimer compounds B4A1 and BB14 water-soluble. The PEG–peptide solubilizers provided excellent payload capacities and solubilized the compounds as colloidal aggregates, which showed negligible induction of apoptosis and the ability to disassemble Tau protein aggregates in a DMSO-free in vitro assay with promising DC_{50} values. Whereas the study confirmed the feasibility of rendering non-fluorescent small organic molecules water-soluble, the screening procedure might be expanded to a broad scope of potential lead compounds with unfavorable pharmacological indices.

Acknowledgments

We thank E. Krause and H. Stephanowitz (FMP Berlin, Germany) for MS sequencing and K. Linkert (HU Berlin) and B. Bulic for the synthesis of B4A1. H.G.B. acknowledges funding from the European Research Council under the European Union's 7th Framework Program (FP07-13; ERC Starting Grant "Specifically Interacting Polymers-SIP", ERC 305064), and E.M. thanks the BMBF (Kompetenznetz für neurodegenerative Demenzen) and the Wellcome Trust/MRC.

Keywords: Alzheimer's disease · bioconjugates · combinatorial screening · precision polymers · Tau protein

How to cite: *Angew. Chem. Int. Ed.* **2016**, *55*, 8752–8756
Angew. Chem. **2016**, *128*, 8894–8899

[1] C. A. Lipinski, F. Lombardo, B. W. Dominy, P. J. Feeney, *Adv. Drug Delivery Rev.* **2001**, *46*, 3.
[2] S. Dunne, B. Shannon, C. Dunne, W. Cullen, *BMC Pharmacol. Toxicol.* **2013**, *14*, 1.
[3] a) J.-H. Zhang, T. D. Y. Chung, K. R. Oldenburg, *J. Biomol. Screening* **1999**, *4*, 67; b) T. Kennedy, *Drug Discovery Today* **1997**, *2*, 436.
[4] S. M. Paul, D. S. Mytelka, C. T. Dunwiddie, C. C. Persinger, B. H. Munos, S. R. Lindborg, A. L. Schacht, *Nat. Rev. Drug Discovery* **2010**, *9*, 203.
[5] a) A. Beig, J. M. Miller, A. Dahan, *Eur. J. Pharm. Biopharm.* **2012**, *81*, 386; b) M. E. Herbig, D.-H. Evers, *Eur. J. Pharm. Biopharm.* **2013**, *85*, 158.
[6] A. Tjernberg, N. Markova, W. J. Griffiths, D. Hallén, *J. Biomol. Screening* **2006**, *11*, 131.
[7] a) R. Duncan, *Nat. Rev. Drug Discovery* **2003**, *2*, 347; b) Y. Bae, S. Fukushima, A. Harada, K. Kataoka, *Angew. Chem. Int. Ed.* **2003**, *42*, 4640; *Angew. Chem.* **2003**, *115*, 4788; c) M. R. Radowski, A. Shukla, H. von Berlepsch, C. Bottcher, G. Pickaert, H. Rehage, R. Haag, *Angew. Chem. Int. Ed.* **2007**, *46*, 1265; *Angew. Chem.* **2007**, *119*, 1287; d) W. B. Liechty, D. R. Kryscio, B. V. Slaughter, N. A. Peppas, *Annu. Rev. Chem. Biomol. Eng.* **2010**, *1*, 149; e) D. Peer, J. M. Karp, S. Hong, O. C. Farokhzad, R. Margalit, R. Langer, *Nat. Nanotechnol.* **2007**, *2*, 751; f) D. Huesmann, A. Sevenich, B. Weber, M. Barz, *Polymer* **2015**, *67*, 240; g) A. V. Kabanov, V. Y. Alakhov, *Crit. Rev. Ther. Drug Carrier Syst.* **2002**, *19*, 1; h) R. Luxenhofer, Y. Han, A. Schulz, J. Tong, Z. He, A. V. Kabanov, R. Jordan, *Macromol. Rapid Commun.* **2012**, *33*, 1613; i) K. Knop, R. Hoogenboom, D. Fischer, U. S. Schubert, *Angew. Chem. Int. Ed.* **2010**, *49*, 6288; *Angew. Chem.* **2010**, *122*, 6430; j) T. Steinbach, F. R. Wurm, *Angew. Chem. Int. Ed.* **2015**, *54*, 6098; *Angew. Chem.* **2015**, *127*, 6196.
[8] A. K. H. Hirsch, F. Diederich, M. Antonietti, H. G. Borner, *Soft Matter* **2010**, *6*, 88.
[9] a) M. Danial, M. J. Root, H.-A. Klok, *Biomacromolecules* **2012**, *13*, 1438; b) L. Hartmann, H. G. Börner, *Adv. Mater.* **2009**, *21*, 3425; c) D. Schaffert, C. Troiber, E. E. Salcher, T. Fröhlich, I. Martin, N. Badgujar, C. Dohmen, D. Edinger, R. Kläger, G. Maiwald, K. Farkasova, S. Seeber, K. Jahn-Hofmann, P. Hadwiger, E. Wagner, *Angew. Chem. Int. Ed.* **2011**, *50*, 8986; *Angew. Chem.* **2011**, *123*, 9149; d) J. V. Georgieva, R. P. Brinkhuis, K. Stojanov, C. Weijers, H. Zuilhof, F. Rutjes, D. Hoekstra, J. C. M. van Hest, I. S. Zuhorn, *Angew. Chem. Int. Ed.* **2012**, *51*, 8339; *Angew. Chem.* **2012**, *124*, 8464; e) K. Hiltebrandt, T. Pauloehrl, J. P. Blinco, K. Linkert, H. G. Börner, C. Barner-Kowollik, *Angew. Chem. Int. Ed.* **2015**, *54*, 2838; *Angew. Chem.* **2015**, *127*, 2880; f) T. Schwemmer, J. Baumgartner, D. Faivre, H. G. Börner, *J. Am. Chem. Soc.* **2012**, *134*, 2385.
[10] S. Wieczorek, E. Krause, S. Hackbarth, B. Röder, A. K. H. Hirsch, H. G. Börner, *J. Am. Chem. Soc.* **2013**, *135*, 1711.
[11] S. Wieczorek, S. Vigne, T. Masini, D. Ponader, L. Hartmann, A. K. H. Hirsch, H. G. Börner, *Macromol. Biosci.* **2015**, *15*, 82.
[12] I. Khlistunova, J. Biernat, Y. P. Wang, M. Pickhardt, M. von Bergen, Z. Gazova, E. Mandelkow, *J. Biol. Chem.* **2006**, *281*, 1205.
[13] a) A. Sydow, A. Van der Jeugd, F. Zheng, T. Ahmed, D. Balschun, O. Petrova, D. Drexler, L. Zhou, G. Rune, E. Mandelkow, R. D'Hooge, C. Alzheimer, E.-M. Mandelkow, *J. Mol. Neurosci.* **2011**, *45*, 432; b) C. Fatouros, G. J. Pir, J. Biernat, S. P. Koushika, E. Mandelkow, E.-M. Mandelkow, E. Schmidt, R. Baumeister, *Hum. Mol. Genet.* **2012**, *21*, 3587.
[14] S. Salomone, F. Caraci, G. M. Leggio, J. Fedotova, F. Drago, *Br. J. Clin. Pharmacol.* **2012**, *73*, 504.
[15] a) Y. Hong-Qi, S. Zhi-Kun, C. Sheng-Di, *Transl. Neurodegener.* **2012**, *1*, 21; b) B. Bulic, M. Pickhardt, E.-M. Mandelkow, E. Mandelkow, *Neuropharmacology* **2010**, *59*, 276.
[16] a) B. Bulic, M. Pickhardt, I. Khlistunova, J. Biernat, E.-M. Mandelkow, E. Mandelkow, H. Waldmann, *Angew. Chem. Int. Ed.* **2007**, *46*, 9215; *Angew. Chem.* **2007**, *119*, 9375; b) M. Pickhardt, G. Larbig, I. Khlistunova, A. Coksezen, B. Meyer, E.-M. Mandelkow, B. Schmidt, E. Mandelkow, *Biochemistry* **2007**, *46*, 10016.
[17] A. Pickhardt, J. Biemat, I. Khlistunova, Y.-P. Wang, Z. Gazova, E.-M. Mandelkow, E. Mandelkow, *Curr. Alz. Res.* **2007**, *4*, 397.
[18] K. S. Lam, S. E. Salmon, E. M. Hersh, V. J. Hruby, W. M. Kazmierski, R. J. Knapp, *Nature* **1991**, *354*, 82.
[19] M. M. Kubota, B. L. Sacco, D. C. Bento, H. de Santana, *Spectrochim. Acta Part A* **2015**, *151*, 80.
[20] J.-F. Lutz, H. G. Börner, *Prog. Polym. Sci.* **2008**, *33*, 1.
[21] C. L. Burnett, B. Heldreth, W. F. Bergfeld, D. V. Belsito, R. A. Hill, C. D. Klaassen, D. C. Liebler, J. G. Marks, R. C. J. Shank, T. J. Slaga, P. W. Snyder, F. A. Andersen, *Int. J. Toxicol.* **2014**, *33*, 13S.
[22] M. Pickhardt, M. von Bergen, Z. Gazova, A. Hascher, J. Biernat, E.-M. Mandelkow, E. Mandelkow, *Curr. Alzheimer Res.* **2005**, *2*, 219.

Received: February 1, 2016
Published online: June 10, 2016

